ARTICLES
https://doi.org/10.1038/s41567-018-0210-0

nature physics

Harnessing electro-optic correlations in an efficient mechanical converter

A. P. Higginbotham[1,2,3,5], P. S. Burns[1,2,5]*, M. D. Urmey[1,2,5], R. W. Peterson[1,2], N. S. Kampel[1,2], B. M. Brubaker[1,2,3], G. Smith[1,2,4], K. W. Lehnert[1,2,3] and C. A. Regal[1,2]

An optical network of superconducting quantum bits (qubits) is an appealing platform for quantum communication and distributed quantum computing, but developing a quantum-compatible link between the microwave and optical domains remains an outstanding challenge. Operating at $T<100$ mK temperatures, as required for quantum electrical circuits, we demonstrate a mechanically mediated microwave–optical converter with 47% conversion efficiency, and use a classical feed-forward protocol to reduce added noise to 38 photons. The feed-forward protocol harnesses our discovery that noise emitted from the two converter output ports is strongly correlated because both outputs record thermal motion of the same mechanical mode. We also discuss a quantum feed-forward protocol that, given high system efficiencies, would allow quantum information to be transferred even when thermal phonons enter the mechanical element faster than the electro-optic conversion rate.

A quantum network entangling spatially separated quantum nodes would permit secure communication and distributed quantum computing[1–4]. Propagating optical fields are the natural choice for quantum links in such a network, as they enable entanglement distribution at room temperature and over kilometre-scale distances. The fast-paced development of superconducting quantum processors[5,6] suggests that the most powerful nodes will use microwave-frequency excitations in ultralow-temperature environments ($T<100$ mK), implying that a quantum-state-preserving electro-optic converter is a crucial element needed for a future quantum internet. Prospective conversion technologies under investigation are ultracold atoms[7,8], optically active spins in solids[9–12], magnons[13], electro-optic materials[14–16] and mechanical resonators[17–19]. To date, there has been no successful demonstration of an electro-optic converter capable of quantum operation. Recent realizations have demonstrated improved capacity for classical signal recovery, albeit at elevated operating temperatures[17–21].

Realizing a quantum electro-optic converter is a challenging task because it entails bringing together superconducting quantum circuits and laser light in an ultralow-temperature environment. The potential for quantum operation can be delineated via two metrics: the bidirectional efficiency between the microwave and optical ports, and the added noise of the converter N_{add}[18,22–24]. In a mechanical converter, low added noise requires high electromechanical and optomechanical cooperativities[23,25], which have yet to be achieved together in a single device. Alternatives to high cooperativity have been explored in other optomechanical systems; in particular, feedback damping has been experimentally shown to ease cooperativity requirements in individual platforms[26–32]. However, quantum electro-optic conversion studies have to date focused on reaching the threshold $N_{add}<1$, at which point arbitrarily low efficiency can be tolerated using quantum repeater concepts that herald the creation of entanglement probabilistically[33].

Here, we explore electro-optic conversion in an alternative feed-forward framework where quantum tasks could be performed even if thermal–mechanical noise yields $N_{add}>1$, provided threshold efficiencies are reached. We demonstrate an unprecedented conversion efficiency of 47 ± 1% in a micromechanical device operated at $T<100$ mK, and implement a feed-forward protocol that exploits noise correlations between the two converter output ports to reduce added noise to $N_{add}=38$ photons. These figures of merit represent significant technical progress relative to the 8% efficiency and 1,500 photons of added noise achieved in a prototype system operated at 4 K[18]. Furthermore, while we focus on electro-optic converters here, our feed-forward protocol is broadly applicable to two-mode signal processing devices in which transmission occurs through a noisy intermediary mode. It also complements recent theoretical work proposing adaptive control for quantum transducers[34,35].

We will consider classical and quantum feed-forward protocols in a microwave–mechanical–optical converter in which the mechanical element is thermally occupied (Fig. 1a). The noise emitted from each port contains a redundant record of the mechanical oscillator's thermally driven motion. During operation, the signal to be converted is injected into the microwave port and an ancilla state is injected into the optical port. The upconverted signal, with noise added, is emitted from the optical port. The ancilla state, contaminated with the same added noise, is emitted from the microwave port. Measuring the downconverted ancilla and feeding forward to the propagating optical mode can remove this correlated added noise.

Classical and quantum feed-forward protocols are distinguished by the choice of ancilla. Simply choosing the ancilla to be optical vacuum causes zero-point fluctuations (vacuum noise) to be fed forward along with the thermal noise. In this case, although thermal noise may be completely removed, vacuum noise from the ancilla is necessarily written onto the upconverted signal. Choosing vacuum as the ancilla therefore prohibits upconversion of a state with negative Wigner function or squeezing, so we refer to it as classical feed-forward. Classical feed-forward is a resource for recovering classical signals, whose performance— interestingly—depends on system efficiencies rather than temperature, quality factor or cooperativity. However, classical feed-forward is apparently unhelpful for quantum tasks.

[1]JILA, University of Colorado and NIST, Boulder, CO, USA. [2]Department of Physics, University of Colorado, Boulder, CO, USA. [3]National Institute of Standards and Technology (NIST), Boulder, CO, USA. [4]Center for Theory of Quantum Matter, University of Colorado, Boulder, CO, USA. [5]These authors contributed equally: A. P. Higginbotham, P. S. Burns, M. D. Urmey. *e-mail: peter.s.burns@colorado.edu

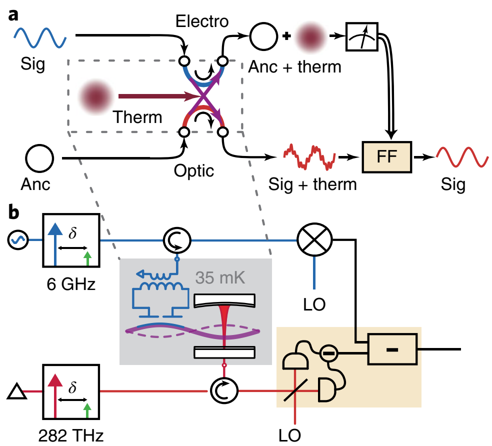

Fig. 1 | Feed-forward schematic and measurement network. a, A signal incident on the microwave port (blue sinusoid) is output from the optical port (red sinusoid) with thermal noise coupled in from the internal port (maroon disc). The optical ancilla (black circle) is simultaneously downconverted with correlated noise added. The ancilla is measured and a feed-forward protocol (FF) is applied. The dotted line is the converter box. The blue and red paths show microwave and optical reflections, and the purple arrows show the conversion process. **b**, Simultaneous coupling of microwave (blue) and optical (red) resonators to a single mechanical mode (purple). Strong optical (red arrow) or microwave (blue arrow) pumps are applied to create optomechanical interaction. A weak probe signal (green arrow) detuned from the pump by δ can be applied to one converter port and detected at the other. The converter box is shaded grey. Feed-forward operations are indicated by beige-shaded regions. For our classical demonstration, these operations are optical heterodyne measurement and subtraction in post-processing. The corresponding operation in a quantum feed-forward protocol would be a unitary displacement of the optical field conditioned on the microwave measurement result.

A different choice of ancilla would allow quantum tasks to be accomplished, even in the presence of thermal noise. For example, if the ancilla is an infinitely squeezed vacuum state, one quadrature can be fed forward noiselessly, permitting noiseless measurement of a single upconverted quadrature or upconversion of a squeezed quadrature without high cooperativity. This quantum protocol does however place limits on measurement and converter efficiencies, as any loss will add noise to the feed-forward process. In the limit of perfect measurement efficiencies and squeezing, a converter efficiency $\eta > 50\%$ is still required to upconvert a squeezed quadrature or measure a remotely prepared microwave quadrature with added noise less than vacuum. We therefore refer to 50% as a quantum threshold efficiency for feed-forward protocols. More sophisticated tasks can be imagined with quantum feed-forward, albeit with more stringent efficiency requirements. In particular, quantum feed-forward could be used to upconvert a qubit state given a qubit encoding robust to noise in one quadrature. One example of such a feed-forward-based qubit upconversion scheme is explored in the Supplementary Information.

Here, we focus on the experimental identification of correlations that allow feed-forward, and perform classical feed-forward with a vacuum ancilla. For this demonstration, we measure both converter outputs in heterodyne detection and perform subtraction in post-processing to remove the correlated noise (Fig. 1b). A quantum protocol would instead entail homodyne measurement of the ancilla at the microwave port, and conditional unitary displacement at the optical port[36].

Our electro-optic converter is housed in a cryostat with base temperature $T=35\,\mathrm{mK}$, and comprises microwave and optical cavities simultaneously coupled to a single vibrational mode of a suspended dielectric membrane with resonant frequency $\omega_m/2\pi = f_m = 1.473\,\mathrm{MHz}$ (Fig. 1b). Strong red-detuned pump tones incident on both cavities parametrically couple mechanical motion to propagating microwave and optical fields at rates $\Gamma_{e,o}$ that greatly exceed the intrinsic mechanical damping rate $\gamma_m = 2\pi\times 11\,\mathrm{Hz}$ (see Methods). Along with the two pump tones, a weak probe tone, incident on either the microwave or optical cavity, is measured in heterodyne detection, and used for characterization and implementation of classical feed-forward.

The converter box is characterized by a series of probe-tone scattering parameter measurements $S_{ij}(\delta)$, where $i=\mathrm{e},\mathrm{o}$ is the measured port, $j=\mathrm{e},\mathrm{o}$ is the excited port and δ is the frequency of the probe relative to the pump[18]. As shown in Fig. 2a, when $\Gamma_e \approx \Gamma_o$, a dip in microwave reflection occurs near $\delta/2\pi = f_m$, with a corresponding peak in microwave-to-optical transmission, indicating the absorption of signals in the microwave port and their emission at the optical port. A nearly identical optical-to-microwave transmission signal is also observed. The peak transmission $|t|^2 = 0.55$ corresponds to a conversion efficiency of $\eta = |t|^2/\mathcal{A} = 0.41$, where $\mathcal{A}$ is the independently measured converter gain due to imperfect sideband resolution[18]. The converter bandwidth (measured as the full-width at half-maximum of the transmission peak) is given by the total linewidth of the optomechanically and electromechanically damped membrane mode, $\Gamma_T = \Gamma_e + \Gamma_o + \gamma_m$.

For comparison, if Γ_e is decreased such that $\Gamma_e \ll \Gamma_o$, microwave reflection becomes almost flat, with a value determined by the microwave cavity coupling, and nearly zero power is transmitted. At the same time, a peak is observed in optical reflection resulting from optomechanically induced transparency effects. The peak height exceeds 1 due to converter gain (see Supplementary Information). The optical reflection peak is suppressed when $\Gamma_e \approx \Gamma_o$, constituting electromechanically induced optical absorption, which, to our knowledge, has not been previously reported.

To further explore the converter box's performance, the efficiency is extracted from peak transmission for a range of Γ_e with $\Gamma_o = 2\pi\times 725\,\mathrm{Hz}$ fixed (Fig. 2b). For fixed optical cavity parameters, efficiency is maximized when damping rates are matched ($\Gamma_e = \Gamma_o$, $\Gamma_T = 2\pi\times 1.45\,\mathrm{kHz}$). The conversion efficiency is fitted to[18]

$$\eta = \frac{4\Gamma_e\Gamma_o}{(\Gamma_e+\Gamma_o+\gamma_m)^2}\eta_M = \frac{4(\Gamma_T-\Gamma_o-\gamma_m)\Gamma_o}{\Gamma_T^2}\eta_M \tag{1}$$

where γ_m and Γ_o are fixed from independent measurements and η_M is the only fit parameter. For our converter $\Gamma_e, \Gamma_o \gg \gamma_m$, and thus $\eta = \eta_M$ when the converter is matched. Therefore, we refer to η_M as the matched efficiency. In this low mechanical dissipation regime, there is negligible energy loss in the electro-optic transduction process itself, but some energy is absorbed in each electromagnetic resonator, and the spatial profile of the optical cavity mode does not perfectly match that of the external modes used for measurement and signal injection (see Supplementary Information). We thus expect $\eta_M = \epsilon(\kappa_{ex,o}/\kappa_o)(\kappa_{ex,e}/\kappa_e)$, where κ_o and $\kappa_{ex,o}$ (κ_e and $\kappa_{ex,e}$) are the optical (microwave) cavity linewidth and external coupling respectively, and ϵ parameterizes the optical cavity mode matching. The fit result, $\eta_M = 43\pm 1\%$, agrees with the theoretical expectation, $\eta_M = 43\pm 4\%$ obtained from independent measurements of ϵ, $\kappa_{ex,o}/\kappa_o$ and $\kappa_{ex,e}/\kappa_e$.

Tuning the membrane position in situ within the optical cavity changes both $\kappa_{ex,o}$ and κ_o due to interference effects (see Supplementary Information), and therefore alters the matched conversion efficiency (Fig. 2c). Matched conversion efficiency initially increases with κ_o, reaching a maximum at $\kappa_o = 2\pi\times 2.7\,\mathrm{MHz}$, and then decreases as internal optical cavity loss begins to dominate. The in situ tuning of the optical cavity also changes the

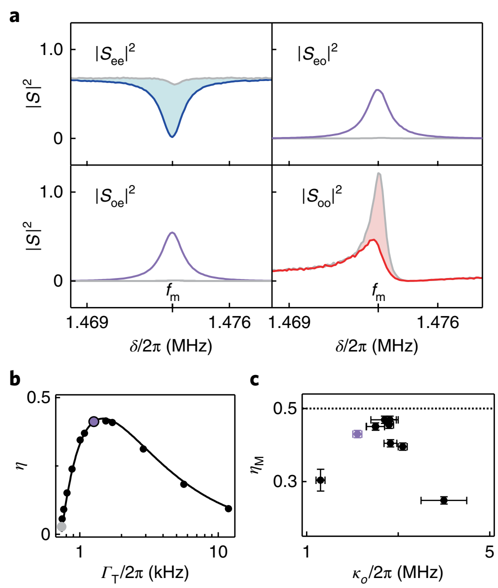

Fig. 2 | Converter efficiency. **a**, Measured converter scattering parameters versus probe frequency δ: microwave reflection (S_{ee}), optical reflection (S_{oo}), microwave-to-optical transmission (S_{oe}) and optical-to-microwave transmission (S_{eo}). The coloured trace is $\Gamma_e \approx \Gamma_o$ (see Methods).The grey trace is $\Gamma_e \ll \Gamma_o$, with the same Γ_o. The shaded region highlights induced absorption of incident power when conversion rates are matched. **b**, Converter efficiency η versus total damping Γ_T. Γ_T is swept by tuning Γ_e with Γ_o fixed. The black line is a fit to equation (1). The purple and grey points correspond to data in **a**. **c**, Matched efficiency η_M versus optical cavity linewidth κ_o. The ratio of external optical cavity coupling to internal loss varies with κ_o. The black dotted line indicates the quantum feed-forward threshold at $\eta_M = 0.5$, discussed in the main text. The horizontal error bars represent the standard deviation of several repeated linewidth measurements. The vertical error bars are obtained by propagating standard error in individual scattering parameter measurements.

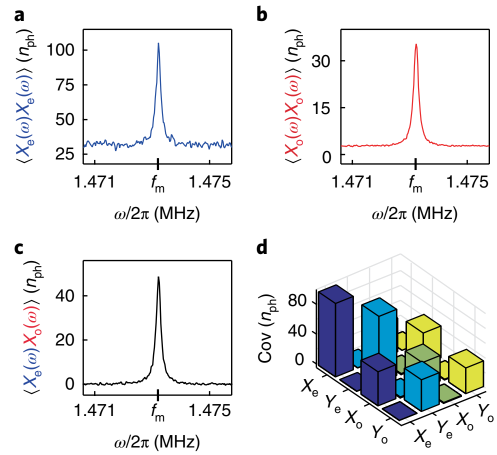

Fig. 3 | Electro-optic correlations. **a**, Microwave real spectral density, $\langle X_e(\omega)X_e(\omega)\rangle$, in units of photons referred to converter output, showing the thermal–mechanical noise peak and background noise from the microwave measurement chain. **b**, The optical real spectral density, $\langle X_o(\omega)X_o(\omega)\rangle$, exhibits similar features. **c**, Real cross-spectral density, $\langle X_e(\omega)X_o(\omega)\rangle$, illustrating that thermal noise exhibits perfect classical correlations between outputs and background noise is uncorrelated. **d**, Covariance matrix obtained from averaging the spectral and cross-spectral densities around ω_m with a $2\pi\times50$ Hz bandwidth, indicating similar behaviour for the imaginary microwave and optical spectral densities and the imaginary cross-spectral density; no correlations exist between real and imaginary parts.

optomechanical coupling and thus the achievable converter bandwidth Γ_T. For intermediate linewidths near the highest efficiencies, the optical cavity became unstable, possibly due to large optomechanical coupling in these regions. The peak conversion efficiency achieved was $47\pm1\%$, approaching the quantum feed-forward threshold efficiency. At peak conversion efficiency, the matched converter bandwidth was 12 kHz, while a 100 kHz bandwidth was achieved at $\kappa_o = 2\pi\times3$ MHz.

During the conversion process, vibrational noise is added to the signal. To explore correlations in this noise, we turn off the weak probe tone and return to a high-stability configuration with $\eta_M = 43\%$, but smaller pump power ($\Gamma_e \approx \Gamma_o$, $\Gamma_T = 2\pi\times200$ Hz). In this configuration, electro/optomechanical cooling of the mechanical mode is diminished, while still maintaining $\Gamma_e, \Gamma_o \gg \gamma_m$. We perform heterodyne measurements of the noise exiting both converter ports (see Supplementary Information), and analyse the results in the frequency domain: $X(\omega)$ and $Y(\omega)$ will denote, respectively, the real and imaginary parts of the Fourier transform of the noise time stream at detuning $+\omega$ from the pump. The total power spectral density is then $S(\omega) = \langle X^2(\omega)\rangle + \langle Y^2(\omega)\rangle$, and is reported in units of photons s^{-1} Hz^{-1}, or more simply photons, referred to the converter output. For example, an ideal heterodyne measurement of $S(\omega)$ gives a background noise level of 1 photon, and 50% loss in the measurement chain would double the background level.

The microwave real power spectral density, $\langle X_e(\omega)X_e(\omega)\rangle$, exhibits a peak of width $\Gamma_T/2\pi = 200$ Hz around $\omega/2\pi = f_m$ (Fig. 3a). The peak height relative to background, $\langle (X_e^{(th)})^2\rangle = 69.2$ photons, is obtained from a Lorentzian fit to the data and attributed to thermally driven mechanical motion at a bath temperature $T = 87\pm4$ mK (see Supplementary Information), which exceeds the cryostat base temperature of 35 mK. The elevated membrane temperature is consistent with independently measured optical heating (see Supplementary Information). The background noise level, 31.8 photons, corresponds to $n_e = 29.6$ photons from vacuum noise and the added noise of the microwave measurement chain, with the remaining 2.2 photons due primarily to parameter noise in the LC circuit (independently calibrated, see Supplementary Information).

The optical real spectral density, $\langle X_o(\omega)X_o(\omega)\rangle$, shows a similar peak (Fig. 3b). The peak height above noise, $\langle (X_o^{(th)})^2\rangle = 33.1$ photons, provides a second measure of the bath temperature, $T = 80\pm4$ mK, consistent with Fig. 3a. The background noise, $n_o = 2.7$ photons, corresponds to vacuum noise plus the effect of loss in the optical measurement chain. Note that $n_o < n_e$, indicating that the optical measurement apparatus is closer to ideal.

The real cross-spectral density, $\langle X_e(\omega)X_o(\omega)\rangle$, has a 47.7 photon peak at $\omega/2\pi = f_m$, indicating that the thermal fluctuations are common to both outputs (Fig. 3c). The difference between the observed correlations and their maximum classical value, $\langle X_eX_o\rangle - \sqrt{\langle (X_e^{(th)})^2\rangle}\sqrt{\langle (X_o^{(th)})^2\rangle} = -0.2\pm0.3$ photons, is consistent with zero, indicating that thermal noise is perfectly correlated between the two outputs, as expected from optomechanical theory (see Supplementary Information). Away from mechanical resonance, the cross-correlation vanishes, as expected for uncorrelated noise from the independent measurement chains. Similar behaviour is observed for $\langle Y_e(\omega)Y_o(\omega)\rangle$ (Fig. 3d).

Harnessing the observed correlations, we use classical feed-forward to recover a weak upconverted signal. With the weak signal incident on the microwave port and detuned from the pump by $\delta/2\pi = f_m + 5$ Hz, microwave reflection and converter transmission to the optical port are simultaneously measured. The microwave reflection is fed forward to remove noise from the upconverted optical signal. In a quadrature picture (see Supplementary Information)

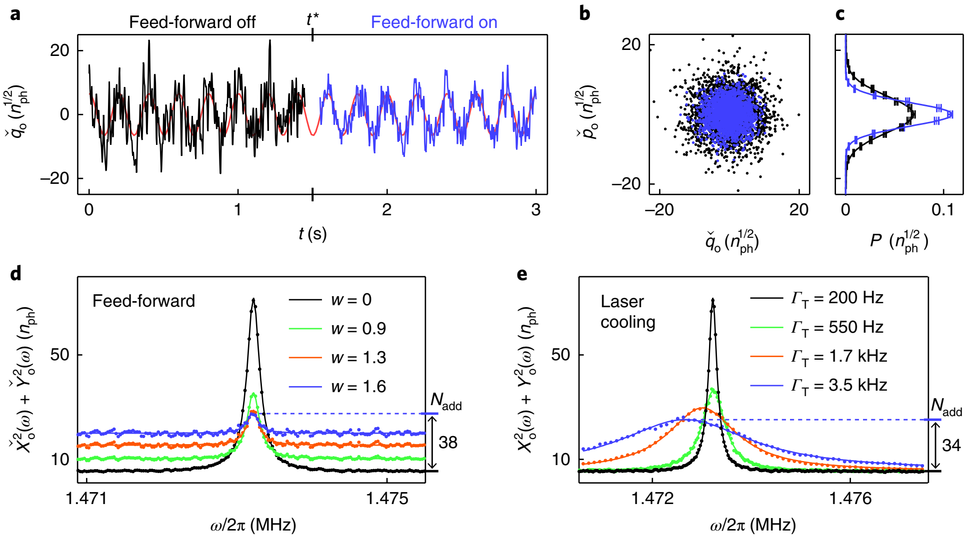

Fig. 4 | Feed-forward operation of a microwave–mechanical–optical converter. a, Fed-forward optical quadrature q_o versus time with feed-forward off ($t < t^*$) and feed-forward on ($t > t^*$). A weak signal incident on the microwave port is recovered at the optical port. **b**, Repeated measurements of both optical quadratures (q_o, p_o) with and without feed-forward. The signal tone is turned off. **c**, $P(p_o)$, the inferred probability density of p_o, with and without feed-forward, with Gaussian fits. The variance decreases by 59% with feed-forward on. The error bars are obtained from Poisson counting statistics. **d**, Total noise power spectra, $X_o^2(\omega) + Y_o^2(\omega)$, for different feed-forward weights, w, with $\Gamma_T = 2\pi \times 200$ Hz. Best added noise in photons referred to converter input, N_{add}, is indicated on the right axis. **e**, Total noise power spectra, $X_o^2(\omega) + Y_o^2(\omega)$, for different laser cooling rates, Γ_T, while maintaining $\Gamma_e \approx \Gamma_o$. Best added noise in photons referred to converter input, N_{add}, is indicated on the right axis.

where demodulated microwave and optical fields are described in the time domain by $(q(t), p(t))$ position-momentum pairs, the fed-forward optical quadrature q_o is given by

$$q_o = q_o - w\sqrt{\frac{n_o}{n_e}}\, q_e \qquad (2)$$

where q_o is the measured optical quadrature, q_e is the microwave quadrature and w is the feed-forward weight; a similar definition is used for p.

Initially, with feed-forward turned off ($w = 0$ for $t < t^*$), the upconverted signal, a $2\pi \times 5$ Hz quadrature oscillation, is difficult to resolve (Fig. 4a). After feed-forward is turned on ($w = 1.6$ for $t > t^*$), the weak signal becomes clearly visible. To quantify the improvement, the optical quadratures (q_o, p_o) are repeatedly measured without a signal tone, as shown in Fig. 4b. The quadratures are Gaussian distributed (Fig. 4c), and feed-forward reduces each quadrature variance by 59%.

Feed-forward performance is limited mainly by the addition of uncorrelated noise from imperfect measurement chains. This limitation can be understood by examining the power spectral density of the feed-forward signal, $\langle X_o^2 \rangle + \langle Y_o^2 \rangle$, where

$$\left\langle X_o^2 \right\rangle = \left\langle X_o^2 \right\rangle + w^2 \frac{n_o}{n_e} \left\langle X_e^2 \right\rangle - 2w\sqrt{\frac{n_o}{n_e}} \left\langle X_e X_o \right\rangle \qquad (3)$$

$$\left\langle Y_o^2 \right\rangle = \left\langle Y_o^2 \right\rangle + w^2 \frac{n_o}{n_e} \left\langle Y_e^2 \right\rangle - 2w\sqrt{\frac{n_o}{n_e}} \left\langle Y_e Y_o \right\rangle \qquad (4)$$

in terms of the measured real and imaginary spectral densities. As shown in Fig. 4d, as the feed-forward weight w is increased, the peak noise power near f_m decreases due to the presence of correlations near mechanical resonance. However, Fig. 4d also illustrates that the noise power off resonance increases with increasing w. At $w = 1$, the background noise receives equal contributions from the optical measurement noise and fed-forward noise from the microwave measurement chain; for $w > 1$, the noise introduced by feed-forward will dominate off resonance while the thermal noise around f_m continues to decrease.

For reporting noise performance of the converter, the relevant metric is noise referred to converter input, which can be calculated from the output noise on resonance by dividing by the apparent converter efficiency, $\mathcal{A} \times \eta$. One can then consider an added feed-forward noise at converter input (right side of Fig. 4d), reflecting how much the observed noise exceeds the amount due to the imperfect measurement chains and vacuum noise. Feed-forward with $w = 1.6$ effectively adds $N_{add} = 38$ photons of noise to the converter input, the majority of which is fed-forward microwave measurement noise.

It is interesting to make a comparison between feed-forward operation and laser cooling (electro/optomechanical damping) of the mechanical oscillator. As shown in Fig. 4e, increasing the total damping, Γ_T, while maintaining matching, $\Gamma_e \approx \Gamma_o$, improves noise performance while increasing bandwidth. Damping rates are limited by laser-induced heating of the superconductor and LC parameter noise (see Supplementary Information). Laser cooling achieved a best value of $N_{add} = 34$ photons of input-referred added noise (right side of Fig. 4e), comparable to the best feed-forward performance. Unlike feed-forward operation, laser cooling does not affect the background noise.

Although feed-forward and laser cooling achieve comparable noise performance in the current set-up, their limitations are quite different. In the presence of technical noise that limits damping rates, the performance of laser cooling is set by $n_{th,m}\gamma_m$, where $n_{th,m}$ is the thermal phonon occupancy of the membrane. Indeed, we have studied laser cooling in a different converter with 10 times lower mechanical dissipation but a lower conversion efficiency of 12%, and achieved an $N_{add} = 13$ photons of added noise. With feed-forward, on the other hand, one can always completely eliminate the effect of thermal noise at the expense of feeding forward measurement noise. Provided $\Gamma_e, \Gamma_o \gg \gamma_m$, feed-forward performance is determined solely by the measurement apparatus, rather than coupling to the thermal bath. It should be emphasized that, for any low-frequency mechanical mode, this is a much less stringent condition on damping rates than high cooperativity ($\Gamma_e, \Gamma_o \gg n_{th,m}\gamma_m$). For example, in a 4 K experiment with a similar measurement set-up, one would expect feed-forward performance similar to that observed here, but laser cooling to be orders of magnitude less effective.

Looking ahead to quantum feed-forward operation, a central challenge is improving microwave and optical measurement performance. In particular, the microwave measurement noise could be improved by using a quantum-limited microwave amplifier[37]. Meanwhile, more theoretical work is needed to thoroughly explore the electro-optomechanical correlations identified here, and to study optimal qubit encodings for microwave–optical conversion with feed-forward.

Methods

Methods, including statements of data availability and any associated accession codes and references, are available at https://doi.org/10.1038/s41567-018-0210-0.

Received: 8 November 2017; Accepted: 12 June 2018;
Published online: 16 July 2018

References

1. Cirac, J. I., Zoller, P., Kimble, H. J. & Mabuchi, H. Quantum state transfer and entanglement distribution among distant nodes in a quantum network. *Phys. Rev. Lett.* **78**, 3221–3224 (1997).
2. Ekert, A. K. Quantum cryptography based on Bell's theorem. *Phys. Rev. Lett.* **67**, 661–663 (1991).
3. Cirac, J. I., Ekert, A. K., Huelga, S. F. & Macchiavello, C. Distributed quantum computation over noisy channels. *Phys. Rev. A* **59**, 4249–4254 (1999).
4. Dür, W. & Briegel, H.-J. Entanglement purification for quantum computation. *Phys. Rev. Lett.* **90**, 067901 (2003).
5. Kelly, J., Barends, R., Fowler, A. G., Megrant, A. & Jeffrey, E. State preservation by repetitive error detection in a superconducting quantum circuit. *Nature* **519**, 66–69 (2015).
6. Ofek, N. et al. Extending the lifetime of a quantum bit with error correction in superconducting circuits. *Nature* **536**, 441–445 (2016).
7. Verdú, J. et al. Strong magnetic coupling of an ultracold gas to a superconducting waveguide cavity. *Phys. Rev. Lett.* **103**, 043603 (2009).
8. Hafezi, M. et al. Atomic interface between microwave and optical photons. *Phys. Rev. A* **85**, 020302 (2012).
9. Imamoglu, A. Cavity QED based on collective magnetic dipole coupling: Spin ensembles as hybrid two-level systems. *Phys. Rev. Lett.* **102**, 083602 (2009).
10. Marcos, D. et al. Coupling nitrogen-vacancy centers in diamond to superconducting flux qubits. *Phys. Rev. Lett.* **105**, 210501 (2010).
11. Kubo, Y. et al. Strong coupling of a spin ensemble to a superconducting resonator. *Phys. Rev. Lett.* **105**, 140502 (2010).
12. Williamson, L. A., Chen, Y.-H. & Longdell, J. J. Magneto-optic modulator with unit quantum efficiency. *Phys. Rev. Lett.* **113**, 203601 (2014).
13. Hisatomi, R. et al. Bidirectional conversion between microwave and light via ferromagnetic magnons. *Phys. Rev. B* **93**, 174427 (2016).
14. Ilchenko, V. S., Savchenkov, A. A., Matsko, A. B. & Maleki, L. Whispering-gallery-mode electro-optic modulator and photonic microwave receiver. *J. Opt. Soc. Am. B* **20**, 333–342 (2003).
15. Xiong, C., Pernice, W. H. P. & Tang, H. X. Low-loss, silicon integrated, aluminum nitride photonic circuits and their use for electro-optic signal processing. *Nano Lett.* **12**, 3562–3568 (2012).
16. Rueda, A. et al. Efficient microwave to optical photon conversion: an electro-optical realization. *Optica* **3**, 597–604 (2016).
17. Bochmann, J., Vainsencher, A., Awschalom, D. D. & Cleland, A. N. Nanomechanical coupling between microwave and optical photons. *Nat. Phys.* **9**, 712–716 (2013).
18. Andrews, R. W. et al. Bidirectional and efficient conversion between microwave and optical light. *Nat. Phys.* **10**, 321–326 (2014).
19. Vainsencher, A., Satzinger, K. J., Peairs, G. A. & Cleland, A. N. Bi-directional conversion between microwave and optical frequencies in a piezoelectric optomechanical device. *Appl. Phys. Lett.* **109**, 033107 (2016).
20. Bagci, T. et al. Optical detection of radio waves through a nanomechanical transducer. *Nature* **507**, 81–85 (2014).
21. Takeda, K. et al. Electro-mechano-optical detection of nuclear magnetic resonance. *Optica* **5**, 152–158 (2018).
22. Safavi-Naeini, A. H. & Painter, O. Proposal for an optomechanical traveling wave phonon–photon translator. *New J. Phys.* **13**, 013017 (2011).
23. Hill, J. T., Safavi-Naeini, A. H., Chan, J. & Painter, O. Coherent optical wavelength conversion via cavity optomechanics. *Nat. Commun.* **3**, 1196 (2012).
24. Zeuthen, E., Schliesser, A., Sørensen, A. S. & Taylor, J. M. Figures of merit for quantum transducers. Preprint at http://arxiv.org/abs/1610.01099 (2016).
25. Safavi-Naeini, A. H. & Painter, O. Design of optomechanical cavities and waveguides on a simultaneous bandgap phononic-photonic crystal slab. *Opt. Express* **18**, 14926–14943 (2010).
26. Cohadon, P. F., Heidmann, A. & Pinard, M. Cooling of a mirror by radiation pressure. *Phys. Rev. Lett.* **83**, 3174–3177 (1999).
27. Arcizet, O. et al. High-sensitivity optical monitoring of a micromechanical resonator with a quantum-limited optomechanical sensor. *Phys. Rev. Lett.* **97**, 133601 (2006).
28. Poggio, M., Degen, C. L., Mamin, H. J. & Rugar, D. Feedback cooling of a cantilever's fundamental mode below 5 mK. *Phys. Rev. Lett.* **99**, 017201 (2007).
29. Genes, C., Vitali, D., Tombesi, P., Gigan, S. & Aspelmeyer, M. Ground-state cooling of a micromechanical oscillator: Comparing cold damping and cavity-assisted cooling schemes. *Phys. Rev. A* **77**, 033804 (2008).
30. Wilson, D. J. et al. Measurement-based control of a mechanical oscillator at its thermal decoherence rate. *Nature* **524**, 325–329 (2015).
31. Rossi, M. et al. Enhancing sideband cooling by feedback-controlled light. *Phys. Rev. Lett.* **119**, 123603 (2017).
32. Rossi, M., Mason, D., Chen, J., Tsaturyan, Y. & Schliesser, A. Measurement-based quantum control of mechanical motion. Preprint at http://arxiv.org/abs/1805.05087 (2018).
33. Duan, L.-M., Lukin, M. D., Cirac, I. & Zoller, P. Long distance quantum communication with atomic ensembles and linear optics. *Nature* **414**, 413–418 (2001).
34. Rakhubovsky, A. A., Vostrosablin, N. & Filip, R. Squeezer-based pulsed optomechanical interface. *Phys. Rev. A* **93**, 033813 (2016).
35. Zhang, M., Zou, C.-L. & Jiang, L. Quantum transduction with adaptive control. *Phys. Rev. Lett.* **120**, 020502 (2018).
36. Braunstein, S. L. & Kimble, H. J. Teleportation of continuous quantum variables. *Phys. Rev. Lett.* **80**, 869–872 (1998).
37. Teufel, J. D., Donner, T., Castellanos-Beltran, M. A., Harlow, J. W. & Lehnert, K. W. Nanomechanical motion measured with an imprecision below that at the standard quantum limit. *Nat. Nanotech.* **4**, 820–823 (2009).

Acknowledgements

We thank J. Thompson and M. Holland for fruitful conversations and K. Cicak for assistance with device fabrication. We acknowledge funding from AFOSR MURI grant number FA9550-15-1-0015, the NSF under grant number PHYS 1734006, DURIP and AFOSR PECASE.

Author contributions

A.P.H., P.S.B. and M.D.U. conducted the experiment and analysed data. A.P.H, P.S.B., M.D.U., R.W.P. and N.S.K. designed and constructed the measurement network. M.D.U and R.W.P. designed and constructed the optical cavity. P.S.B. designed and fabricated the flip-chip device. A.P.H. and G.S. developed feed-forward theory. A.P.H., P.S.B., M.D.U., B.M.B., G.S., K.W.L. and C.A.R. wrote the manuscript. C.A.R. and K.W.L. supervised the work. All authors commented on the results and manuscript.

Competing interests

The authors declare no competing interests.

Additional information

Supplementary information is available for this paper at https://doi.org/10.1038/s41567-018-0210-0.

Reprints and permissions information is available at www.nature.com/reprints.

Correspondence and requests for materials should be addressed to P.S.B.

Publisher's note: Springer Nature remains neutral with regard to jurisdictional claims in published maps and institutional affiliations.

Methods

Device parameters. We realize an electro-optic converter by simultaneously coupling microwave and optical resonators to a single mode of a mechanical oscillator. The mechanical oscillator is a thin, suspended dielectric membrane, with resonant frequency $\omega_m/2\pi = f_m = 1.473$ MHz for the mode of interest. A portion of the membrane is metallized and arranged as a mechanically compliant capacitor in a superconducting LC circuit, with resonant frequency $\omega_e/2\pi = 6.16$ GHz and linewidth $\kappa_e = 2\pi \times 2.5$ MHz. Another portion of the membrane is situated in the mode of a Fabry–Perot optical cavity with resonant frequency $\omega_o/2\pi = 281.8$ THz and linewidth $\kappa_o = 2\pi \times 2.1$ MHz. Vibrational motion of the membrane modulates ω_e by $G_e \approx 2\pi \times 8$ MHz nm^{-1} and ω_o by $G_o \approx 2\pi \times 13$ MHz nm^{-1}. The entire assembly is housed in a cryostat with base temperature $T = 35$ mK[38], where both microwave and optical modes are close to their quantum ground state.

With a strong red-detuned pump beam incident on the optical cavity, the optomechanical interaction couples the mechanical oscillator to propagating optical fields at a rate Γ_o that exceeds the intrinsic mechanical damping rate $\gamma_m = 2\pi \times 11$ Hz. At pump detuning $\Delta_o = -\omega_m$ and in the resolved sideband limit ($4\omega_m/\kappa_o \gg 1$), the optomechanical damping rate has the simple form[18]

$$\Gamma_o = \frac{4G_o^2 x_{zp}^2 \alpha_o^2}{\kappa_o} \quad (5)$$

where α_o is the intracavity pump amplitude and x_{zp} is the zero-point amplitude of the membrane mode. The electromechancial damping in the presence of a strong red-detuned microwave pump tone has the same form:

$$\Gamma_e = \frac{4G_e^2 x_{zp}^2 \alpha_e^2}{\kappa_e} \quad (6)$$

In practice, our converter is moderately sideband-resolved ($4\omega_m/\kappa_o \approx 4\omega_m/\kappa_e \approx 2.5$), with pump detunings $\Delta_e/2\pi = -1.47$ MHz and $\Delta_o/2\pi = -1.11$ MHz. These details change the precise form of the expressions for Γ_o and Γ_e but not the essential physics.

We set the optical pump detuning Δ_o to maximize the optomechanical damping rate per incident photon. In the resolved sideband limit, this maximum damping occurs at $\Delta_o = -\omega_m$, but this is not generally the case with imperfect sideband resolution.

Fabrication details. The mechanical oscillator is a 100-nm-thick, 500-μm-wide silicon nitride membrane suspended from a silicon chip. A 25-nm-thick niobium film that serves as one capacitor pad is fabricated on one quadrant of the membrane before it is released. The membrane chip is flipped over and affixed to a second silicon chip, on which a microfabricated niobium circuit comprising an inductor and a second capacitor pad was previously patterned using standard lithographic techniques. The full fabrication process has been described elsewhere[39]. The flip-chip assembly is constructed with a West Bond manual die bonder, and the chips are affixed using Stycast 2850. In the fully assembled flip-chip device, the two niobium pads form a parallel-plate capacitor with a plate spacing of 300 nm, and the 6.16 GHz resonant frequency of the resulting LC circuit is modulated by vibrations of mode of interest. Propagating microwaves are wirelessly coupled to the LC circuit through a re-entrant microwave cavity, which also holds mirrors that form a Fabry–Perot optical cavity with a 281.8 THz resonant frequency[40]. The optical cavity comprises two mirrors, with 29 ppm and 98 ppm power transmission respectively, separated by 2.6 mm. The chip assembly is placed in the standing wave of the optical cavity with the membrane 750 μm from the high-transmission mirror, such that the membrane's vibrations modulate the cavity's resonant frequency[41]. The optical mode intersects the membrane in the quadrant opposite the capacitor, and these two regions of the membrane move in phase for the mechanical mode of interest.

Data availability. The data that support the plots within this paper and other findings of this study are available from the corresponding author upon reasonable request.

References

38. Peterson, R. W. et al. Laser cooling of a micromechanical membrane to the quantum backaction limit. *Phys. Rev. Lett.* **116**, 063601 (2016).
39. Andrews, R. W. *Quantum Signal Processing with Mechanical Oscillators*. PhD thesis, Univ. Colorado (2015).
40. Menke, T. et al. Reconfigurable re-entrant cavity for wireless coupling to an electro-optomechanical device. *Rev. Sci. Instrum.* **88**, 094701 (2017).
41. Thompson, J. et al. Strong dispersive coupling of a high-finesse cavity to a micromechanical membrane. *Nature* **452**, 72–75 (2008).